AGU PUBLICATIONS

Water Resources Research

RESEARCH ARTICLE
10.1002/2017WR021365

Key Points:
- Methane leakage from oil-and-gas wellbores below freshwater aquifers impacts groundwater quality
- Multiphase analysis allows study of gas-phase source-zone pressure, capillarity and relative permeability, which influence methane migration
- Multiphase parameters play a fundamental role in determining volumes and flow rates of methane reaching groundwater

Correspondence to:
Amy K. Rice,
amrice@mines.edu

Citation:
Rice, A. K., McCray, J. E., & Singha, K. (2018). Methane leakage from hydrocarbon wellbores into overlying groundwater: Numerical investigation of the multiphase flow processes governing migration. *Water Resources Research*, *54*, 2959–2975. https://doi.org/10.1002/2017WR021365

Received 22 JUN 2017
Accepted 25 FEB 2018
Accepted article online 28 FEB 2018
Published online 19 APR 2018

Methane Leakage From Hydrocarbon Wellbores into Overlying Groundwater: Numerical Investigation of the Multiphase Flow Processes Governing Migration

Amy K. Rice[1], John E. McCray[1,2], and Kamini Singha[1,2,3]

[1]Hydrologic Science and Engineering Program, Colorado School of Mines, Golden, CO, USA, [2]Department of Civil and Environmental Engineering, Colorado School of Mines, Golden, CO, USA, [3]Department of Geology and Geological Engineering, Colorado School of Mines, Golden, CO, USA

Abstract Methane leakage due to compromised hydrocarbon well integrity can lead to impaired groundwater quality. Here we use a three-dimensional, multiphase (vapor and aqueous), multicomponent (methane, water, salt), numerical model (TOUGH2 EOS7C) to investigate hydrogeological conditions that could result in groundwater contamination from natural gas wellbore leakage that migrates upward toward a freshwater aquifer. The conceptual model used for the simulations assumes methane leakage at 20–30 m below groundwater. We perform 180 simulations for a sensitivity analysis, examining (1) multiphase flow parameters related to storage, capillarity, and relative permeability, including porosity (ϕ), initial fluid-phase saturation (S_L), and van Genuchten n and α, (2) geostatistical variations in intrinsic permeability (k_i), and (3) methane source-zone pressure. Simulated mean k_i values are 10^{-18} and 10^{-13} m^2 with variances of 1 and 5 m^4. Simulated source-zone pressures range from just over ambient hydrostatic pressure at the depth of leakage (100 kPa) to the maximum pressure that steel casings are commonly rated to withstand (20,340 kPa). k_i, initial S_L, ϕ, and van Genuchten's n and α were the most important parameters in determining the volume of methane reaching groundwater during a given time period. Multiphase parameterization of formations underlying freshwater aquifers and overlying hydrocarbon production zones is fundamental to assessing aquifer vulnerability to methane leakage.

Plain Language Summary Methane leakage from oil and gas wellbores below freshwater aquifers may impact groundwater quality. The scope of the problem is such that millions of kilograms of methane could reach groundwater in the case of a long-term, persistent leak. However, flow rates at the base of the aquifer are slow, and changes in methane concentrations may go undetected. In this paper, we use numerical modeling to investigate hydrogeological conditions that could result in groundwater contamination from natural-gas wellbore leakage that migrates upward toward a freshwater aquifer. Measurement or careful estimation of parameters impacting both gas- and liquid-phase flow and transport are needed in determining volumes and flow rates of methane reaching groundwater and, thus, aquifer vulnerability to methane leakage.

1. Introduction

The development of directional drilling and stimulation of reservoirs by high-volume hydraulic fracturing ("fracking") makes it economically feasible to recover unconventional hydrocarbon resources from shale formations (e.g., Allouche et al., 2000; Hubbert & Willis, 1957; MIT Energy Initiative, 2011; USDOE, 2009). By 2040, projections indicate that shale-gas production will grow to 29.0 trillion cubic feet—69% of total U.S. dry natural gas production—and natural gas will surpass coal as the United States' largest source of electricity (USEIA, 2015, 2016). The rapid development of hydrocarbon resources from unconventional reservoirs has been accompanied by public concern about potential environmental impacts, including surface water (e.g., Olmstead et al., 2013) and groundwater (e.g., Llewellyn et al., 2015; Osborn et al., 2011). The greatest risk of water contamination is usually attributed to surface spills and poor well integrity (e.g., Gorody, 2012; Jackson et al., 2013; Sherwood et al., 2016; Vengosh et al., 2014; Watson & Bachu, 2009).

Impacts to water quality from hydrocarbon development include the potential for natural gas to reach drinking-water aquifers or surface waters. Methane, the principal component of natural gas, is not considered a health hazard from ingestion. However, an action level of 10 mg/L is suggested by the U.S. Department of the Interior due to combustion hazards (Duncan, 2015; Eltschlager et al., 2001; Vidic et al., 2013). Additionally, oxidation of methane has been linked to changes in groundwater geochemistry, including decreased concentrations of dissolved oxygen, increased pH, and bacterial sulfate reduction (Kelly et al., 1985; Van Stempvoort et al., 2005), especially in confined aquifers (Roy et al., 2016). If uncombusted methane is released to the atmosphere, it can function as a potent greenhouse gas, albeit over a relatively short time scale (e.g., Howarth et al., 2011). Perhaps most important is that gas-phase methane, which is generally conservative with respect to transport, could be a precursor to more hazardous components of natural gas or production fluids. While data indicate that flow of methane has occurred from hydrocarbon wells to freshwater aquifers (e.g., Digiulio & Jackson, 2016; Llewellyn et al., 2015; Osborn et al., 2011; Warner et al., 2012), incomplete information on baseline methane and groundwater geochemistry prior to shale-gas development hinders interpretation of these systems (e.g., Gorody, 2012; Molofsky et al., 2011).

Previous studies have simulated fluid migration from hydrocarbon production zones to freshwater aquifers along permeable pathways, such as abandoned or degraded wells or faults (e.g., Birdsell et al., 2015; Gassiat et al., 2013; Nowamooz et al., 2015; Reagan et al., 2015), where compromised wells and faults are considered fully connecting over the hundreds to thousands of meters separating production zones from groundwater. For leakage to occur, failure of barriers (e.g., steel casing and cement sheath) separating hydrocarbon wells from surrounding media must be assumed. However, it is more realistic to simulate leakage below freshwater aquifers where regulations require fewer barriers. Additionally, there is a lack of data on wellbore methane-leakage rates, so examining a range of source-zone pressures is necessary to investigate the relative importance of leakage rate as compared to porous media and multiphase flow characteristics.

Most previous models of water-quality impacts associated with oil-and-gas development have employed single-phase models (e.g., Birdsell et al., 2015; Brownlow et al., 2016; Gassiat et al., 2013; Myers, 2012). Multiphase analysis is better equipped to describe persistent contamination problems related to methane leakage as compared to single-phase models. For example, gas-phase methane trapped due to stratigraphy could act as a continued source of aqueous-phase methane until the trapped methane is dissolved. Aqueous-phase methane may migrate from a leakage source to a drinking-water well more slowly than expected due to decreased aqueous-phase relative permeability caused by the presence of gas-phase methane in pores. If effective permeability is significantly impacted by increased gas-phase saturation, water-well yield may decline. A few recent studies of water-quality impacts associated with hydrocarbon development explore multiphase techniques (e.g., Kissinger et al., 2013; Nowamooz et al., 2015; Reagan et al., 2015). These studies have focused on uncertainty of permeability and porosity, but not multiphase (i.e., capillary and relative permeability) parameters. Instead, Kissinger et al. (2013) and Nowamooz et al. (2015) apply Leverett scaling to adapt multiphase parameters measured elsewhere to the zones of interest in their models (i.e., formations, fault zones, or annular cement), and Kissinger et al. (2013) alter fault-zone residual gas and liquid saturations. Reagan et al. (2015) highlight the need to investigate variations in capillarity in future work.

Kissinger et al. (2013), Nowamooz et al. (2015), and Reagan et al. (2015) identified multiphase parameters appropriate for a given location; however, parametric variation studies are needed for evaluation of the importance of multiphase parameters in solving/simulating problems of methane migration in the subsurface. Here we investigate methane leakage into low-permeability, unfractured media below a freshwater aquifer with a sensitivity analysis investigating the impact of multiphase parameters in simulating subsurface methane migration. Knowledge of how each parameter impacts the simulations can inform practitioners on which parameters should be measured, or carefully estimated, and which parameters can be set at reasonable or literature values. Measurement of multiphase flow parameters for deep subsurface systems associated with methane leakage is expensive and time-consuming, and has not been done in previous published studies. We view this as a gap in the research.

Our conceptual model is based loosely on the Pierre Shale, which separates the hydrocarbon production zone from groundwater in the Wattenberg Field of the Denver Julesburg Basin, near Denver, Colorado, USA. Use of multiphase analysis allows simulation of nonwetting phase methane gas source-zone pressure, capillarity, and relative permeability (k_{rg}), and consideration of viscosity and density effects associated with

multiple interacting phases. Relative permeability is especially important because its variation, depending on phase saturation, can result in orders of magnitude changes in effective permeability and greatly impact the transport of methane in models. Capillarity is important because it controls the effectiveness of lithological barriers. This is the first study to consider natural gas wellbore leakage using both multiphase analysis and flow through heterogeneous media; we examine the impact of multiphase parameter variation on a two-phase system of methane migration through media partially saturated with brine.

To achieve our objectives, we: (1) gathered publicly available data on intrinsic permeability (k_i) porosity (ϕ), and multiphase saturation of the Pierre Shale and hydraulic-fracturing regulations and practices in the Wattenberg Field; (2) collected k_i, ϕ, and aqueous saturation (S_L) data from oil-and-gas operators active in this region; (3) developed a three-dimensional multiphase, multicomponent numerical model to simulate wellbore leakage of methane below groundwater; and (4) conducted a sensitivity analysis varying source pressure, k_i, ϕ, S_L, and parameters describing capillarity and relative permeability surrounding the simulated leak zone.

2. Geological Context and Conceptual Model

2.1. The Wattenberg Field of Northeastern Colorado

This study is designed to evaluate the relative importance of hydrogeological parameters on methane migration generally, so we do not undertake the massive data collection and model calibration effort that would be necessary to analyze actual leakage potential for any specific region. To link our simulations to a real-world scenario, we based our conceptual model on the Pierre Shale of the Wattenberg Field, in Northeastern Colorado (Figure 1). The Wattenberg Field is a region of intense oil-and-gas activity with 54,000 hydrocarbon wells, approximately 50,000 of which are vertical and the remaining 4,000 are horizontal. The Wattenberg Field produces more gas than oil with 12.6 billion m^3 (446 billion cubic feet) of gas and 14.0 million m^3 (88 million barrels) of oil in 2014 (Sherwood et al., 2016). Over half of vertical wells (developed beginning in the 1970s) and almost all horizontal wells (developed beginning in 2010) are hydraulically fractured (Higley & Cox, 2007; Ladd, 2001; Sherwood et al., 2016).

In the region of the Wattenberg Field, the Pierre Shale overlies the Niobrara Formation and underlies the Laramie-Fox Hills Aquifer, which is lowest aquifer in the Denver Basin Aquifer System (Figure 1). The Pierre Shale is generally fine-grained and largely composed of clay minerals (Schultz et al., 1980). In the area of the Wattenberg Field, it descends approximately 2,000 m from the base of the Fox Hills Aquifer (CGS, n.d.; Higley & Cox, 2007; Robson & Banta, 1995). Regional k_i (estimated on the order of hundreds of kilometers) for the Pierre Shale has been measured as low as 10^{-21} m^2 and as high as 10^{-16} m^2 (Bredehoeft et al., 1983; Neuzil, 1994). Laboratory-scale k_i (estimated on the order of centimeters) has been measured between 10^{-21} and 10^{-18} m^2 (Neuzil, 1994). For discussion of the geologic history of the Denver Basin, readers are referred to Weimer and Sonnenberg (1996), Ladd (2001), and Drake et al. (2014).

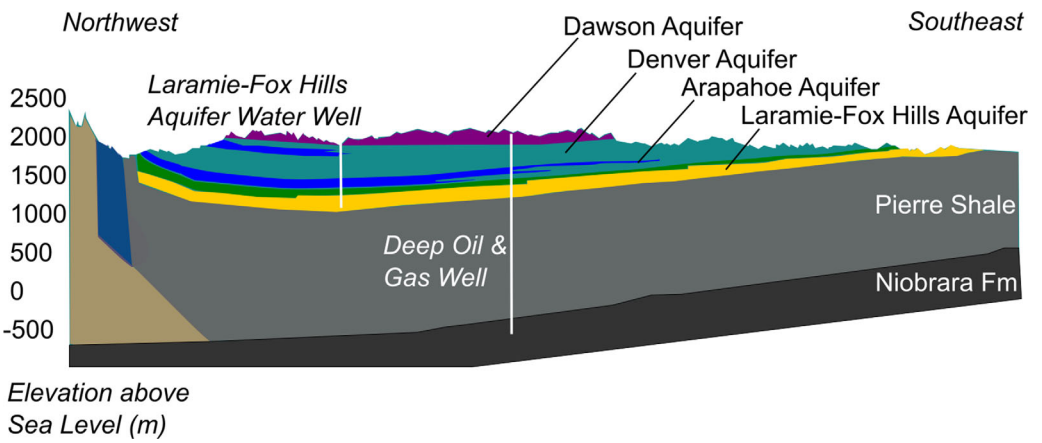

Figure 1. Northwest-southeast cross section showing the Pierre Shale as it overlies the Niobrara Formation and underlies the Denver Basin Aquifer system. Modified from Colorado Geological Survey (CGS) [n.d.]. Cross section length is approximately 100 km.

2.2. Conceptual Model of Wellbore Methane Leakage Into the Pierre Shale

The conceptual model used here is based on a generic natural gas well in the Wattenberg Field. We simulate methane migration over a time scale of 100 years. Previous modeling studies have considered time scales for groundwater contamination associated with natural gas wellbore leakage ranging from 2 years (Reagan et al., 2015) to 30 years (Kissinger et al., 2013) to 100 years (Kissinger et al., 2013; Nowamooz et al., 2015) to greater than 1,000 years (e.g., Gassiat et al., 2013). The studies with shorter time scales examine methane migration whereas longer duration studies tend to focus on transport of hydraulic-fracturing chemicals. Our choice to model for 100 years represents one of the longest timeframes for methane migration studies.

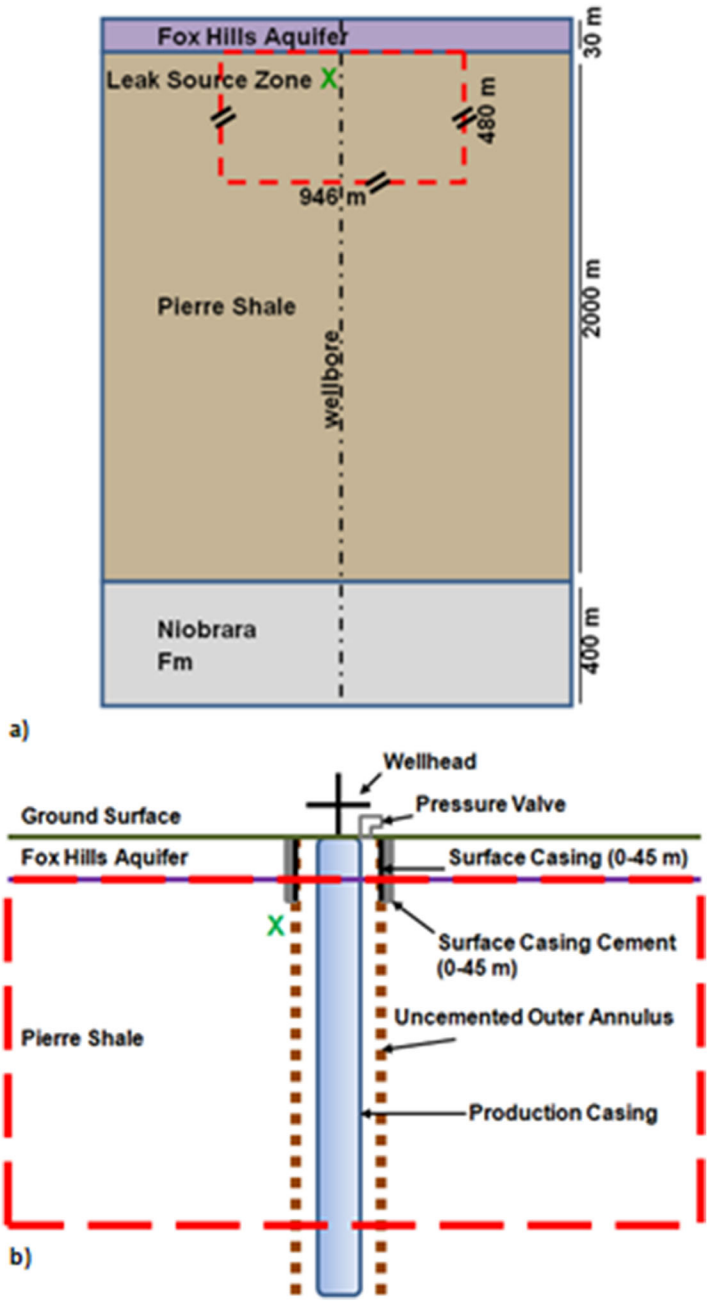

Figure 2. (a) Generalized conceptual model of the Wattenberg Field in vertical cross section. The red dashed box encloses a vertical slice of our three-dimensional our modeled domain. The green X marks where methane leakage occurs in our models. (b) Cross-sectional schematic of a vertical wellbore typical of Wattenberg Field. Not to scale. Major well components are identified to illustrate our choice of leakage depth, which is at the base of a hydrocarbon well surface casing 20–30 m below groundwater, a depth where regulations no longer require steel casing and cement barriers to protect groundwater. The outer annulus marked as uncemented in this figure is legally required to be filled with cement at depths below those shown.

We assume methane leakage occurs 20–30 m below the bottom of groundwater into the Pierre Shale. In Colorado, regulations dictate that the outermost layers of steel casing and cement separating the wellbore from the surrounding formation stop at 15 m (oil-and-gas regulations, commonly in English units, state 50 ft) below the bottom of freshwater aquifers (Figure 2). Our leakage depth of 20–30 m falls below the zone at which the surface casing and cement sheath are no longer required. Regulations require the cementing of production casing 60 m (200 ft) above the shallowest producing hydrocarbon formation. The annular region between the bottom of the surface casing and the top of the production casing cement may be left open (COGCC, 2016). Regulations vary by state, but most require similar protection to minimize the risk of groundwater contamination. Oil-and-gas operators have the option to cement more of the annular space, which has become increasingly common through time in the Wattenberg Field (Stone et al., 2016).

Pressure in the annulus between the surface and production casing typically is monitored by a valve installed at the surface. Colorado state regulations do not allow flaring or venting of methane and other gases from hydrocarbon well annuli to the atmosphere (COGCC, n.d.), so surface-casing vent flows do not occur. Elevated annular pressures are common, and often go unexplained (Lackey et al., 2017). In this work, we assume that methane enters the annular space around the production casing from intermediate formations or has migrated from depth due to inadequate cement above the production zone (e.g., Dusseault et al., 2014) (Figures 2a and 2b). Methane then leaves the annulus at the bottom of the surface casing, 20–30 m below a freshwater aquifer. To simplify analysis, it is assumed that: (1) leakage occurs after active extraction has ceased, (2) the production casing is intact, and leakage into the surrounding formation occurs only from the annular region at the base of the surface casing, and (3) sufficient methane pressures and permeability exist in gas-bearing formations to allow leakage at a steady rate over 100 years. In the Wattenberg Field, testing of annular pressures has not been continuous over 100 years, so it is unclear whether pressures are sustained this long. However, the third assumption is supportable based on the limited data available (e.g., Kang et al., 2016; Lackey et al., 2017). Connections between annular spaces and deeper, pressurized sources of gas may raise and sustain annular pressure. Alternately, variations in annular pressure may be associated with temperature changes. As heat from production fluids is transferred to annular fluids, it temporarily increases pressure, and eventually dissipates. Lackey et al. (2017) describe 48 samples of gas collected by the Colorado Oil and Gas Conservation Commission (COGCC) from the annular space between the

surface casings and production casings in Wattenberg Field. They found that 46 contained thermogenic methane. These results suggest that one or more connections exist between the near-surface annular space and deeper hydrocarbon production zones (e.g., Osborn et al., 2011), which is the more likely scenario for sustained annular pressure as compared to transient temperature effects.

We simulate steady leakage (or source-zone pressure) over 100 years to support our goal of investigating the impact of multiphase flow parameters on subsurface methane migration. Sensitivity to multiphase parameters is evaluated using methane flow rates at the base of an aquifer as sourced from a leaking wellbore. Varying source flow rates or pressure would change flow rates at the base the aquifer, complicating analysis of the influence of multiphase parameters. Nevertheless, a decline in methane source pressure could be expected as leakage continues (e.g., Baihly et al., 2010; Fetkovich et al., 1987). We therefore highlight the first 10 years of leakage, when source pressures are expected to be high relative to later times (e.g., Baihly et al., 2010), with the remainder of the 100 year simulations included to show persistence through time of trends associated with variation of multiphase parameters.

3. Numerical Simulation of Methane Migration

3.1. Numerical Simulator

The numerical studies were performed using the TOUGH2 simulator (Pruess & Moridis, 2012), with fluid property equation-of-state module EOS7C. The EOS7C module analyzes five mass components: water, brine, methane, tracer, and a noncondensable gas. The gas phase in the simulations was composed of methane and water vapor, with vapor-pressure lowering as per the Kelvin equation, allowing variation in the water vapor mass fraction as a function of capillary pressure (Pruess et al., 2012). Peng-Robinson equations-of-state (Peng & Robinson, 1976) were used to calculate gas density, enthalpy, and viscosity, with an assumption of local equilibrium between phases. Movement of vapor-phase and aqueous-phase components occurred by Fickian diffusion and a multiphase, density-dependent formulation of Darcy's Law (Oldenburg et al., 2004). Use of Darcy's Law can result in an underestimation of gas flow due to "slip flow," or the tendency of gases to have nonzero velocity at pore walls (e.g., Scanlon et al., 2002). Therefore, we include the Klinkenberg effect in our simulations with a value of the Klinkenberg parameter ($b = 1E6\ Pa^{-1}$) appropriate for shale (Wu et al., 1998). The model domain is within the Pierre Shale and has dimensions of 946 × 946 × 1,058 m, including upper boundary elements, which are discussed below; the underlying Niobrara Formation is not included in this numerical model. The elevation defined as $z = 0$ is at the top of the Pierre Shale (Figure 3), coinciding with the bottom of a freshwater aquifer in our conceptual model. The leak source zone is located at the lateral center of the domain between $z = -20$ and -30 m (i.e., 20–30 m below the base of the freshwater aquifer). The model domain is discretized with 127,832 elements (58 × 58 × 38 elements of variable size in the x, y, and z directions, respectively). A subdomain comprising a region 500 × 500 × 250 m surrounds the leak source zone; elements in this zone are cubes 10 m on each side, with a total of 62,500 cells. Homogeneous cell sizes were maintained in the zone surrounding the leak to support simple introduction of geostatistical k_i variation, as described below. We conducted a sensitivity analysis to ensure that these cells were of sufficient resolution; making them smaller did not impact methane flow reaching the base of the aquifer. Grid Peclet numbers near the methane source were ≈2 in the x directions and y directions and ≈5 in the z direction. Outside of the leak source zone, element length scales approximately doubled for each new cell added in the x, y, and z directions, with a maximum aspect ratio of 9. In preliminary models, aspect ratios >10 were observed to increase computational expense by increasing model convergence times. The bottom of our model is defined as −480 m, or 480 m below groundwater.

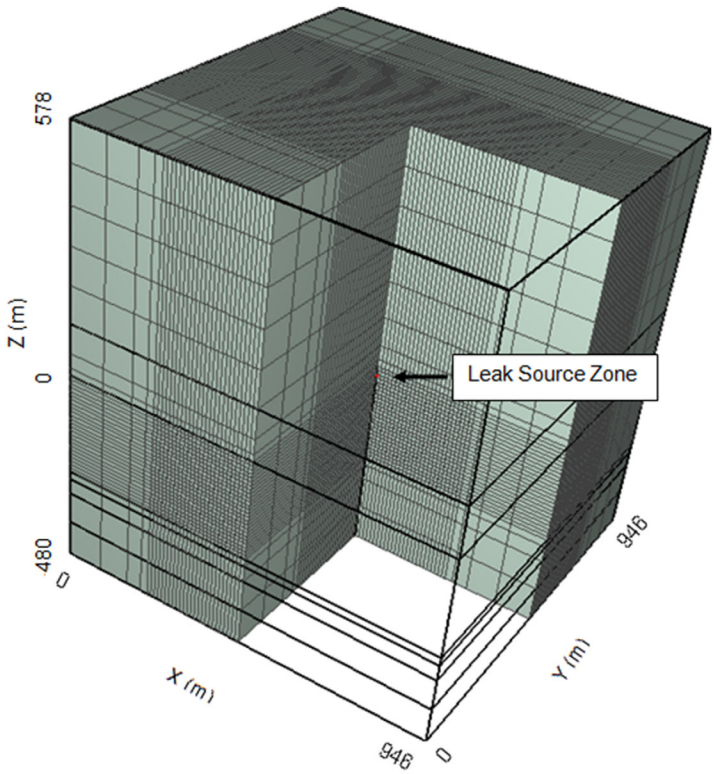

Figure 3. Numerical grid used for simulation. The cutaway shows finer discretization in the center of the model, which is near the leakage source zone.

Table 1
Pierre Shale Parameters and Model Boundary Conditions

Parameters	Value/Equation	Comment/Reference
Initial gas saturation	0.4	K. Tanner (personal communication, 7 October 2015)
Initial Pressure	8.2E4 Pa	Calculated hydrostatic pressure at the base of the Fox Hills aquifer in the region of Wattenberg Field
Brine density at STP	1185.1 kg m^{-3}	Oldenburg et al. (2004)
Porosity, ϕ	0.08	Neuzil (1994) and K. Tanner (personal communication, 7 October 2015)
van Genuchten parameter, λ (***n***)[a]	0.499 (2.00)	Neuzil (1994) and Huet et al. (2005)
van Genuchten parameter, $1/P_0$ (α)*	3.83E-9 (3.76E-5 cm^{-1})	Neuzil (1994) and Huet et al. (2005)
Residual water saturation, S_{lr}	0.2	Based on typical maximum gas saturations reported for shales, e.g., Séjourné et al. (2013) (in Nowamooz et al., 2015)
Residual gas saturation, S_{gr}	1.0E-4	i.e., negligible
Tortuosity model; $\mathbf{S_\beta}$ refers to the saturation of a given phase, β	$\tau_0\tau_\beta = \phi^{1/3}S_\beta^{10/3}$	Millington and Quirk (1961)
Diffusion coefficient of methane in the liquid phase, D_l^m	1.0E-9 m^2 s^{-1}	Pruess et al. (2012)
Diffusion coefficient of water in the gas phase, D_g^w	1.0E-5 m^2 s^{-1}	Pruess et al. (2016)
Klinkenberg parameter	1.0E6 Pa^{-1}	Klinkenberg (1941), Wu et al. (1998), Tanikawa and Shimamoto (2006), and Wang and Reed (2009)
Aquifer temperature (top)	12°C	USEPA (2016)
Geothermal gradient dT/dz	−0.0465°C m^{-1}	Higley and Cox (2007)
Thermal conductivity	2.0 W m^{-1} K^{-1}	Robertson (1988) and Pruess et al. (2012)
Boundary Conditions		
Top	Liquid phase: fixed pressure (8.2E4 Pa) Vapor phase: fixed saturation (0.404)	
Bottom	No-flow boundary	
Lateral boundaries	No-flow boundary	

[a]Values of van Genuchten parameters are input to TOUGH2 as λ and $1/P_0$, but due to the common usage of n and α, these values are also printed here. The relationships are $\lambda = m = 1 - 1/n$ and $1/P_0 = \alpha/\rho g$.

3.2. Boundary Conditions

The boundary conditions used for the simulations are presented in Table 1. Elements above $z = 0$ serve as boundary elements. They are included in the model to generate conditions similar to a multiphase Cauchy boundary condition, which was not available in TOUGH2 EOS7C, at the base of the aquifer ($z = 0$), where liquid-phase and vapor-phase flow out of the domain are a function of both liquid-phase and vapor-phase head and flow. The top boundary condition at $z = 578$ m is set as constant liquid-phase pressure and constant gas saturation. A sensitivity analysis was conducted to set this distance, as defined by the distance required from the base of the freshwater aquifer to top boundary that would allow flow of methane unconstrained by the top boundary condition for 100 years. Pressure at the top boundary was defined to achieve hydrostatic pressure at the base of the freshwater aquifer.

The low ϕ and k_i of the Pierre Shale (Table 1) allow for slow advection and diffusion of liquid-phase materials, and the natural potential gradient of the vapor phase tends upward due to density-driven flow. Therefore, no vapor-phase or liquid-phase flow is expected at the bottom of the modeled domain. The lower boundary condition could have been prescribed as either constant pressure equal to the initial pressure for the liquid phase and constant saturation for the vapor phase or no-flow for both phases. Simulations conducted with constant pressure and saturation and no-flow boundary conditions at the base of the model produced negligible changes in flow of both vapor and liquid into the surficial aquifer, so a more computationally efficient no-flow boundary was applied. No-flow boundaries for vapor and liquid were also prescribed at the lateral edges of the domain, following simulations to determine how far away these boundaries needed to be to avoid influencing flow near the source zone.

3.3. Material Properties

Mean k_i, ϕ, and brine saturation are assigned based on reported values for the Pierre Shale (Neuzil, 1994; K. Tanner, personal communication, 7 October 2015). Here we use a relatively conservative value for the

Pierre Shale with a mean k_i of 10^{-18} m^2. Because initial conditions include methane in the pore space, we assume that methane-sorption sites are occupied and sorption is negligible.

A capillary model is defined by relating capillary model parameters to k_i and ϕ (Huet et al., 2005). In our model, capillary pressure and relative permeability are calculated as a function of saturation using the water-retention parameters and saturated hydraulic conductivity of van Genuchten (1980) and unsaturated hydraulic conductivity parameters based on the pore-size model of Mualem (1976). The Brooks-Corey model, used in the approach of Huet et al. (2005), is not available in TOUGH2 EOS7C, so conversation to van Genuchten parameters was performed using the method of Lenhard et al. (1989). Parameters used to define capillarity and relative permeability in this work are van Genuchten n and α and the residual phase saturations. van Genuchten n is a shape parameter relatable to pore-size distribution (e.g., Freeze & Cherry, 1979). The parameter n occurs in both the capillary-pressure functions and the relative-permeability model (Table 1 and equations (1a) and (2a), below).

The capillary-pressure function is:

$$P_{cap} = -\left(\frac{1}{\alpha}\right)\left(\left([S_*]^{-\frac{1}{1-\frac{1}{n}}}\right)-1\right)^{-1/n} \tag{1a}$$

where

$$S_* = \frac{S_l - S_{lr}}{S_{ls} - S_{lr}} \tag{1b}$$

The relative-permeability model is:

$$k_{rl} = S_*^{0.5}\left(1-\left(1-S_*^{\frac{1}{1-\frac{1}{n}}}\right)^{1-\frac{1}{n}}\right)^2 \; if \;\; S_l < S_{ls}; 1 \;\; if \;\; S_l > S_{ls} \tag{2a}$$

and

$$k_{rg} = \left(1-S_\#\right)^2\left(1-S_\#^2\right) \tag{2b}$$

with

$$S_\# = \left(S_l - S_{lr}\right)/\left(1-S_{lr}-S_{gr}\right) \tag{2c}$$

where P_{cap} (Pa) is capillary pressure, where $P_{cap} = P_{nw} - P_w$ and where nw = nonwetting phase and w = wetting phase. α (cm^{-1}) and $n(-)$ are van Genuchten parameters. S_* *and* $S_\#$ are mobile-phase saturations. S_{lr} is residual liquid saturation, and S_{ls} is maximum liquid saturation. k_{rl} is relative permeability for the liquid phase, and k_{rg} is relative permeability for the gas phase. S_{gr} is gas-phase residual saturation.

The direct and significant impact of n on multiphase permeability is immediately apparent in equation (2a). Larger values of n are associated with more well-sorted soils, in which most of the soil grains, and therefore most of the pore sizes, fall within a relatively narrow range and thus have higher ϕ than otherwise similar poorly sorted soils. Well-sorted soils also have a more limited range of pressures over which saturation changes occur and a larger second derivative at the inflection points of the pressure-saturation curve (e.g., van Genuchten, 1980). As a result, in multiphase models, soils with larger values of n are more likely to experience pulsed migration of the nonwetting phase (Gorody, 2012). Also, increasing n tends to increase available void space for the nonwetting phase, which results in higher k_{rg}.

The van Genuchten α (equation (1a)) is a scaling parameter related to methane-entry pressure (also called "displacement" or "bubbling" pressure) (Freeze & Cherry, 1979). Lower values of α are associated with higher entry pressure. For the leakage scenarios modeled here, decreasing α effectively makes it more difficult for methane from the leak to displace the aqueous phase. Increased S_L associated with lower α decreases k_{rg}, resulting in a correlative relationship between α and the amount of methane reaching the base of the aquifer. Due to the impact of α on capillarity, this parameter influences the relative strength of the driving force (i.e., multiphase pressures) and of the capillary barrier.

No data were available for irreducible gas or water saturations. In the simulations presented here, vapor-phase saturations increase due to methane leakage. Gas entrapment can occur due to occlusion during

processes that resemble imbibition (i.e., increasing S_L), but gas cannot be trapped during processes that increase vapor-phase saturations. Therefore, residual gas saturation was set to a negligible value of 0.01%. Irreducible water saturation was set at 20% because 80% is the maximum gas-phase saturation used in models of similar formations (e.g., Nowamooz et al., 2015). Subsequent analysis indicated minimal sensitivity to irreducible water saturation.

3.4. Source-Zone Properties

To perform our analyses, it was necessary to define a leak depth (discussed in section 3.2) and a flow rate of methane out of the leak source zone. Leakage was imposed along a line source located in the lateral center of the domain. Methane leaks below aquifers are not uniquely related to the practice of hydraulic fracturing. They also can occur for traditional (vertical, not hydraulically fractured) hydrocarbon wells.

Unconventional wells may leak more often than conventional wells due to structural integrity failure of cement and/or casing barriers intended to separate production fluids and groundwater, which are usually much longer and experience higher pressures (e.g., Ingraffea et al., 2014). However, some evidence suggests that modern regulations decrease the likelihood of leakage from any new well (Stone et al., 2016). Increased annular pressure may not lead to incidents of groundwater contamination, especially in newer hydrocarbon wells (Lackey et al., 2017; Sherwood et al., 2016; Watson & Bachu, 2009).

Determining a rate for hypothetical methane leakage depends on factors such as annulus pressure, formation pressure, formation saturation, formation k_i and relative permeability, and fluid density and viscosity. There is little information in the literature pertaining to field-based measurements of wellbore methane-leakage rates and/or source-zone pressure, although inferences based on annular pressure or surface-casing vent flows provide useful approximations (Roy et al., 2016; Watson & Bachu, 2009). Methane-leakage rates based on numerical modeling studies vary over several orders of magnitude (e.g., Nowamooz et al., 2015; Reagan et al., 2015), depending largely on the conceptual model used and values of parameters such as annular permeability (e.g., Reagan et al., 2015) and production zone permeability (e.g., Nowamooz et al., 2015). As a base-case approximation of the rate at which methane would exit a wellbore at the bottom of the surface casing, we apply the rate published in Nowamooz et al. (2015) for a formation in the St. Lawrence Lowlands of Quebec (Scenario C6), which is 7E-4 kg/s. This study was selected due to its use of three-dimensional multiphase analysis and similarity between their conceptual model and ours, specifically a vertically extensive, low-k_i intervening formation between the hydrocarbon production zone and groundwater. We include a sensitivity analysis to examine how methane source-zone pressures, which influence leakage rates, impact methane flow rates at the base of a freshwater aquifer.

Methane leakage was simulated two ways: constant injection and constant pressure, with rates apportioned by permeability and head (i.e., slight changes in flow occurred with vertical position along the 10 m line source due to difference in head with elevation). Pressure simulations employed a range of source-zone pressures. The lowest was just over ambient pressure at the depth of leakage and the highest corresponded to the maximum pressure for which casings commonly used in the Wattenberg Field are rated (Schlumberger, 2014). The range of pressures simulated here could realistically be encountered in annular spaces in the Wattenberg Field via failures of cemented surface casings, cemented production casings, or annular hydrostatic pressure (e.g., Stone et al., 2016). To define pressure at the source zone, an "extra" cell was added to the model. The extra cell was attached to one of the cells surrounding the line source used for the injection simulations leading to a lateral offset of 7 m from the source zone for the injection simulations. The difference is much smaller than the lateral extent of the computational domain (x, $y = 946$ m) and did not change the amount of methane reaching the base of the aquifer. The volume of the extra cell was 0.3142 m^3 with 0.1 m radius and 10 m in the z direction. Pressure was distributed evenly through the cell, and methane saturation defined at 99.9%, assuming degraded or absent cement in the annular region.

3.5. Treatment of Heterogeneity in K_i

For this study, we used spatially correlated, three-dimensional, random fields to investigate the effects of variations in k_i on groundwater contamination from hydrocarbon wellbore leakage. Heterogeneity was defined in a 500 × 500 × 250 m (x, y, z) zone surrounding the leak source zone. Mean k_i was maintained with no random variation for elements outside the leakage zone. The homogeneous outer elements were

Table 2
Hydrogeological Parameter Values Used in the Pierre Shale and Silt/Layered Clay Sensitivity Analyses

	Pierre Shale (Base Case A)	Lower shale parameter values	Higher shale parameter values	Silt/layered clay (Base Case B)	Sand
Homogeneous k_i (m^2)	1E-18	1E-19[a]	1E-17[a]	1E-13	1E-10
van Genuchten-Mualem λ (−)/n	0.518[b]/2.07	0.493[b]/1.97	0.530/2.13	0.083[c]/1.09	0.627[c]/2.68
van Genuchten $1/P_0$ (Pa^{-1})/α (cm^{-1})	3.55E-6[b]/3.48E-4	4.57E-7[b]/4.48E-5	1.91E-5/1.88E-3	8.15E-5[c]/8.00E-3	1.48E-5[c]/0.145
Initial $_{SL}$ (%)	60	80	40	60	80
ϕ (%)	8	6[a]	20[a]	20	30

[a]These values fall within the range of reported k_i and ϕ for shale (Neuzil, 1994). The method of Huet et al. (2005) is applied to find values for the van Genuchten parameters. [b]No data were available on van Genuchten parameters for the Pierre Shale, so these values were calculated using ϕ and k_i data applying the method of Huet et al. (2005). [c]These values are based on class averages for sand and clay from Schaap et al. (1999).

included to eliminate boundary effects, and because methane from the leakage zone does not reach the outer elements, k_i variation was not needed. The heterogeneous fields were generated with sequential Gaussian simulation using the Geostatistical Software Library (GSLIB) (Deutsch & Journel, 1998). For each value of k_i, 25 distinctly different but equally probable random fields were generated, assuming a log-normal distribution and zero mean which were converted to a mean k_i of 10^{-13} and 10^{-18} m^2 with variances of 1 and 5 m^4 used with each mean. It is common for geostatistical simulations to make use of large ensembles of realizations, often on the order of at least 100 realizations (Goovaerts, 1997). However, large ensembles were not feasible for the computationally intensive simulations presented here; one realization takes on the order of a week of clock-time to process. Other studies with as few as 10–20 geostatistical realizations have demonstrated physically meaningful results with small decreases in uncertainty with additional realizations (e.g., Goovaerts, 1999; Maxwell et al., 2008; Navarre-Sitchler et al., 2013).

3.6. Simulation Strategy

Our sensitivity metric is flow of methane (m^3/d) arriving at the base of the aquifer ($z = 0$) (Figures 5, 6, and 8). The first part of our sensitivity analysis focuses on hydrogeologic characteristics of the porous media, specifically k_i, van Genuchten n and α, initial S_L, and ϕ. Values of parameters were chosen for the Pierre Shale, a silt/layered clay, and a sand to allow application of our model results to common near-surface aquifer materials (Bear, 1972) (Table 2). In general, the minimum values correspond to those of Pierre Shale, except for van Genuchten n, which is lower for the silt/layered clay simulations (Schaap et al., 1999). A total of 20 parameter sensitivity simulations were completed.

The assumption of homogenous k_i was relaxed for the second stage of the sensitivity analysis to investigate how permeability variation, as defined by changes in mean, correlation length, and variance, influence transport of methane from a leaking wellbore to the base of an aquifer. First, a homogeneous model was run with k_i equal to either 10^{-13} or 10^{-18} m^2 everywhere in the domain. Subsurface pressure output from the homogenous simulation was used as the initial condition for simulations where correlated, random variations in k_i were applied to the leakage source zone. Finally, a continuous flow of methane was applied in the leak source zone. Two three-dimensional correlations lengths were used: X, Y = 50 m; Z = 20 m and X, Y = 200 m; Z = 80 m. For each correlation length, a variance of 1 and 5 m^4 was applied. For each combination of correlation length and variance, 25 permeability maps were generated with a mean k_i of 10^{-18} m^2. The simulations with a variance of 1 m^4 were repeated with a mean k_i of 10^{-13} m^2, for a total of 150 simulations.

For the final stage of sensitivity analysis, source-zone pressure was varied. Source-zone pressure-sensitivity simulations used initial conditions that correspond to the Pierre Shale (homogeneous k_i equal to 10^{-18} m^2). Methane pressure was varied in the source zone with the following values: 100, 1,000, 2,500, 5,000, 10,000, 12,500, 15,000, 17,500, and 20,340 kPa.

4. Results and Discussion

In this section, the results of the simulations based on the Pierre Shale are presented first. Then, the results of our sensitivity analyses are presented to examine how transport of methane from a leaking wellbore to a

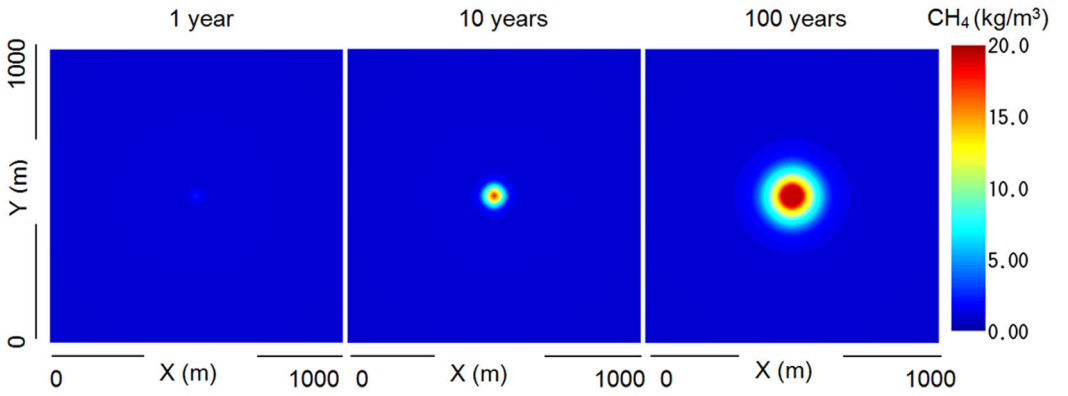

Figure 4. Plan view of methane concentrations at the base of the aquifer at (a) 1 year, (b) 10 years, and (c) 100 years for the homogeneous Pierre Shale scenario.

freshwater aquifer is impacted by (1) changes in multiphase flow parameters related to storage, capillarity, and relative permeability (i.e., ϕ, initial phase saturation, and van Genuchten n and α), (2) variations in matrix k_i, and (3) source-zone pressures and flow rates. Within the unique context of multiphase flow for methane leakage, we evaluate the assumed dominance of k_i over other parameters and explore the impacts of varying source-zone nonwetting phase pressure.

4.1. Pierre Shale Scenario

The Pierre Shale scenario features homogeneous k_i of 10^{-18} m^2 and a source-zone methane flow rate of 7E-4 kg/s (Table 2). Figure 4 shows methane concentration at the base of the aquifer at 1, 10, and 100 years. The plume is laterally symmetrical due to the homogeneous permeability field used in this simulation. The diameter of the plume at the base of the aquifer is approximately 350 m at 100 years. Methane flow rate at the base of the aquifer for this scenario is 44.7 m^3/d at 100 years (Figure 5), with initial flow 0.005 m^3/d and the remainder due to wellbore leakage.

4.2. Sensitivity Analysis

4.2.1. Hydrogeological Characteristics

The most important parameter with respect to methane plume propagation is k_i, as determined by methane flow rate at the base of the aquifer (Figures 5a and 5b). The scenario where the k_i was varied from the silt/layer clay parameter set to the k_i of the Pierre Shale shows a methane flow rate similar to the Pierre Shale scenario (Figure 5b). The flow rate of methane reaching the base of the aquifer is 16.5% different, with the flow rate at 100 years 37.3 m^3/d for the scenario with the same k_i as the Pierre Shale and with silt/layered clay values of ϕ, initial S_L, and van Genuchten parameters.

The influence of van Genuchten n on methane flow rates varies with the base case considered. For the relatively small range in the Pierre Shale sensitivity analysis (Figure 5a and Table 2), the impact of varying n is negligible (green lines for n fall under the black line for the Pierre Shale in Figure 5a). However, there is substantial variation in the methane flow rate when n was varied over a larger range in the higher permeability silt/layered clay scenario. Time to breakthrough and volume of methane reaching groundwater varied with n (Figure 5b) due to the inclusion of n in both the capillary pressure function and relative-permeability model. When only n is varied from the silt/layered clay scenario (e.g., all the parameters are held at the silt/layered clay values and n is given a value in the range of shale), the flow rate at 100 years changes by 9%, with flow rates of 125 m^3/d for the silt/layered clay scenario and 114 m^3/d when n is varied to 2.07.

For the silt/layered clayed sensitivity analyses, the next largest changes in methane flow were associated with variations in initial S_L and ϕ followed by varying van Genuchten α. The Pierre Shale sensitivity analysis shows substantial changes only when initial S_L and ϕ are varied, with compressibility of the gas phase combined with low k_i limiting the impact of lowering S_L on methane flow rates. Values of ϕ are inversely correlated with methane flow rates, which is expected due to increased storage and lower mobile-phase velocities at higher ϕ. Initial S_L is inversely correlated with methane flow rates, which occurs due to

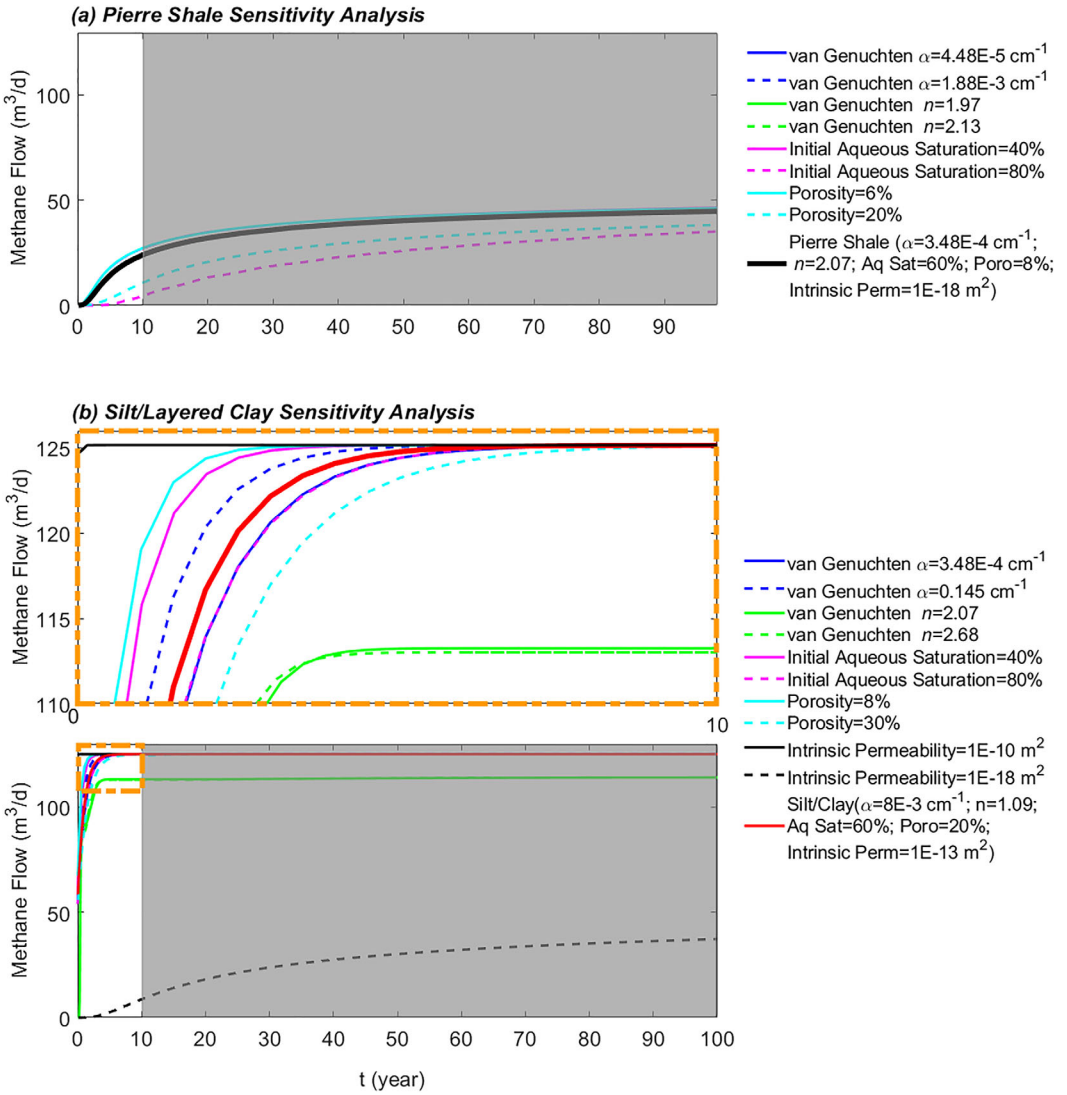

Figure 5. Hydrogeological sensitivity analysis, in which (a) the Pierre Shale is used as the base case and (b) silt/layered clay is used as the base case. For both (a) and (b), volumetric flux of methane at the base of the aquifer for our modeled scenarios is plotted, varying: (i) the capillary pressure/saturation relationship (van Genuchten α and n), (ii) k_{rg} (van Genuchten n), (iii) k_i, (iv) ϕ, and (v) initial S_L. The blow-up panel focuses on methane flow rates at the base of the aquifer for the silt/layered clay base case scenario to show variations in methane flow rates in the first 10 years of the simulations. Methane flow rates for times >10 years after leakage begins are overlain with gray to indicate the low probability of steady leakage occurring for durations >10 years.

decrease in relative permeability for the gas phase when more of the aqueous phase is present (equation (2a)). van Genuchten α is correlated with methane flow rates at the base of the aquifer. Lower values of α require higher methane gas-phase pressure to displace the aqueous phase. The effects of varying α are noticeable in our models at the edges of the plume as methane displaces pore water. Effects of varying α are more prominent at earlier times because the plume grows through time and has a larger surface-area-to-volume ratio early in its migration (Figure 5).

4.2.2. k_i Variation

The results of this part of our sensitivity analysis indicate that the difference between the maximum and minimum flow of methane at the base of the aquifer increases with increasing variance in k_i (Figure 6a versus 6c) and increasing correlation length in k_i (Figure 6a versus 6b and 6c versus 6d). Also, from Figure 6e and 6f, we infer that geostatistical variation in k_i is more of an influential factor on methane transport at lower k_i. Flow rates from cell to cell are more variable as variance in k_i increases, and the flow rate at the base of the aquifer is a composite of these smaller-scale changes. We also find increased variability of methane flow rate with increased correlation length in k_i. Here the correlation lengths in these simulations are

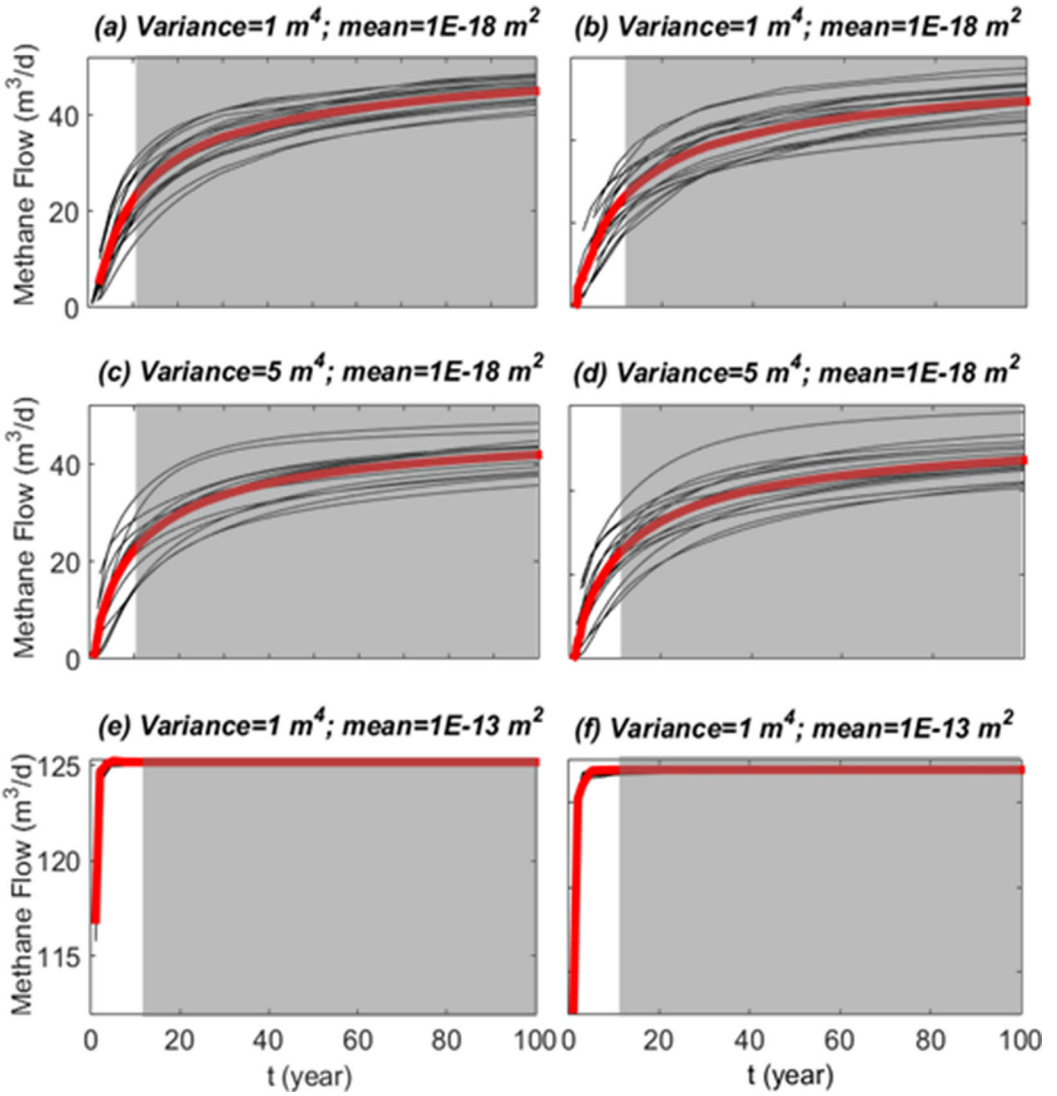

Figure 6. Geostatistical sensitivity analysis. The left-hand column (a, c, and e) shows flow rates from simulations with lower correlation lengths ($C_X = C_Y = 50$ m; $C_Z = 20$ m) than those in the right-hand column (b, d, and f) ($C_X = C_Y = 200$ m; $C_Z = 80$ m). Simulations in the top row include a relatively low variance of 1 m^4 and mean k_i associated with the Pierre Shale (10^{-18} m^2). Simulations in the middle row have a higher variance of 5 m^4 and the same mean k_i as the top row. In the bottom row, variance is the same as the top row, and mean k_i is raised to the value associated with the base-case simulations in Figure 5 (10^{-13} m^2). Twenty-five equally probable correlated random k_i maps were generated and modeled with each of these six scenarios. Black lines represent methane flux at the base of the aquifer associated with a given realization of k_i. Red lines indicate the mean of the realizations shown on the plot. Methane flow rates for times >10 years after leakage begins are overlain with gray to indicate the low probability of steady leakage occurring for durations >10 years.

small enough with respect to the overall grid size that they tend to homogenize k_i, which leads to a tighter clustering around the mean flow rate as compared to simulations with a larger correlation length (Figure 7). The low density and viscosity of methane as compared to water allows homogenization of methane flow rates around the mean at relatively large length. It is necessary to simulate a mobile methane gas phase to see this result; it could not be reached via single (aqueous) phase modeling.

Not surprisingly, shorter k_i correlation lengths lead to a higher methane concentration in the lateral center, and the plume associated with longer k_i correlation lengths has a larger lateral footprint. Comparison between Figures 5 and 6 indicate that k_i variation has a greater impact at the base of the aquifer at later times as compared to variation of van Genuchten α, initial S_L, and ϕ. However, the range of flow rates

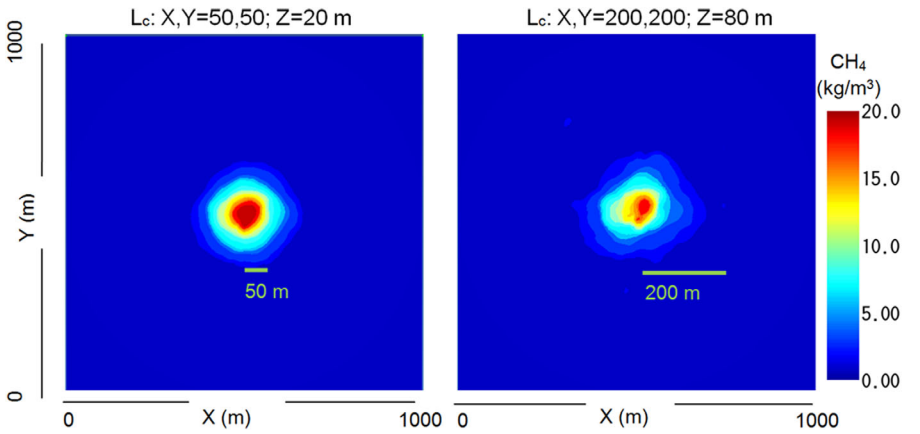

Figure 7. Plan view of methane concentrations at the base of the aquifer at 100 years for one realization of k_i with correlation lengths, L_c (a) X,Y = 50,50; Z = 20 m, and (b) X,Y = 200,200; Z = 80 m.

shown in these plots covers approximately ± 0.17 m^3/d, which is approximately 7 times less than the perturbation in methane flow caused by varying k_i (Figure 5). The implication of this analysis is that having data on k_i and relative permeability of formations underlying freshwater aquifers and overlying hydrocarbon production zones is fundamental to assessing aquifer vulnerability to methane leakage, while information on k_i variation is less critical.

4.2.3. Methane Source Term

The source-term sensitivity analysis indicates that methane flux at the base of the aquifer increases with increasing source-zone pressure, as expected (Figure 8a). For comparison, the injection-based Pierre Shale simulations have a source pressure of 9E3 kPa 20–100 years after leakage begins. The trend in mass reaching the aquifer is approximately linear at higher pressures, but nonlinear below about 1E4 kPa (Figure 8b). In models that include a gas phase, both storage and compression could lead to this effect, in addition to nonlinear behavior associated with capillary pressure and relative-permeability relationships. Our initial condition includes methane present in the pore space, so the nonlinear behavior seen here is due to methane gas compression, associated with increased gas concentration between the leak source and groundwater. Given the same ϕ, gas compression accounts for a greater proportion of the methane leaving a lower-pressure source, which contributes to the observed nonlinear relationship between source strength and mass of methane reaching groundwater (Figure 8b). For all modeled scenarios, methane reaches groundwater in less than 1 year with the volume of methane transferred into the aquifer varying with source pressure. The simulated flow rates of methane into the aquifer are slow and would be difficult to measure in the field (e.g., ISO, 1991). However, wellbore leakage of methane below a freshwater aquifer in these models produces millions of kilograms of methane to be transferred to groundwater (Figure 8b) in the case of persistent long-term leaks. The nonlinear behavior between mass and source-zone pressure indicates that higher pressure source zones pose additional risk to groundwater resources, in part due to the larger lateral extent of methane plumes at the base of the aquifer at higher source pressures (Figure 8c). Besides creating a larger cross section for methane flux, a bigger plume diameter increases opportunity for short-circuit flow of methane to groundwater if connected fractures are present within this range.

5. Conclusions

In these simulations, methane from hydrocarbon wellbore leakage can reach groundwater in less than 1 year assuming low-permeability, unfractured media. Multiphase parameters, i.e., those that influence capillarity and relative permeability, are important for these models: precise parameterization of multiphase processes provides a more accurate conceptual model of methane migration through variably saturated porous media than a single-phase model. Specifically, our results show that consideration of variations in gas-phase pressure and saturation significantly impacts the flow rate and volume of methane reaching groundwater from a leaking natural gas well. k_i is the most important matrix parameter in terms of the

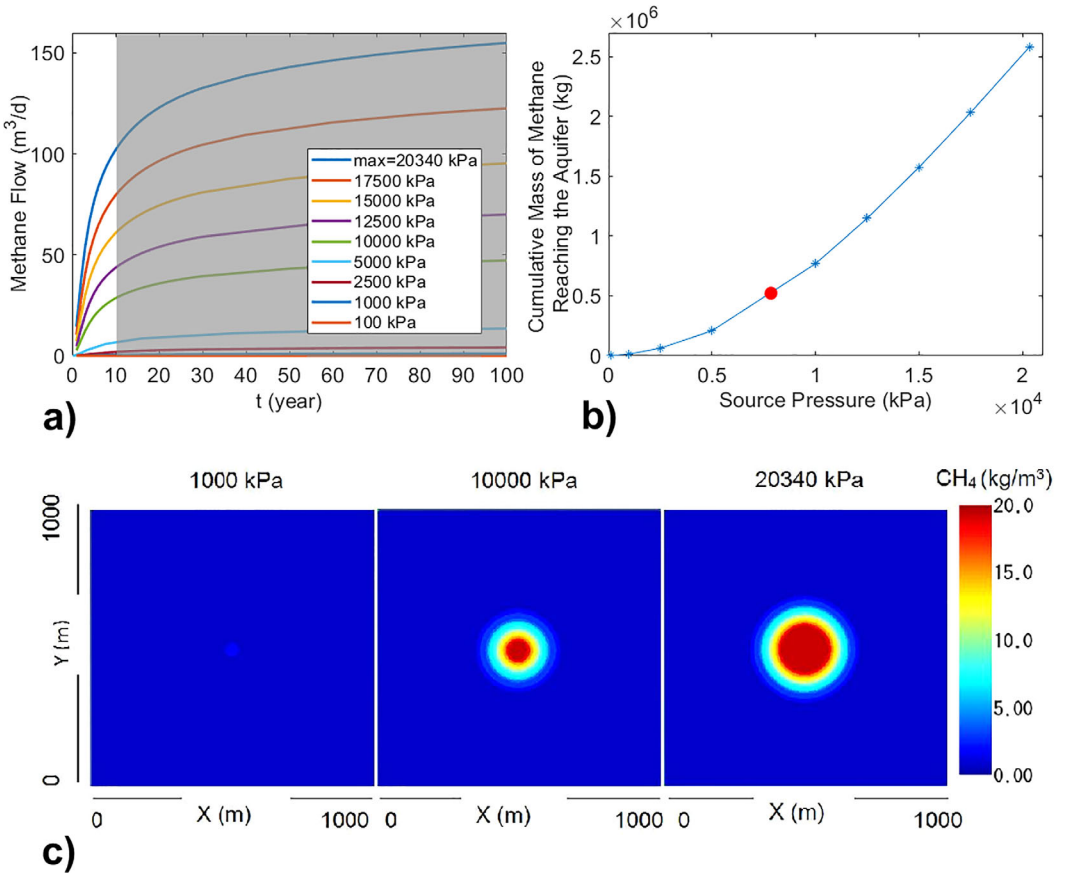

Figure 8. Source-zone sensitivity analysis. (a) Temporal evolution of methane flux at the base of the aquifer for varying source-zone pressurization. Methane flow rates for times >10 years after leakage begins are overlain with gray to indicate the low probability of steady leakage occurring for durations >10 years. (b) Mass of methane reaching the aquifer, summed over the 100 year simulations and plotted against source-zone pressure. The red circle marks the highest annular pressure recorded in the Colorado Oil and Gas Conservation Commission data for the Wattenberg Field. (c) Impact of varying source pressure on the lateral extent of the methane plume at the base of the aquifer at 100 years after leakage begins. On left, methane source pressure just above critical (Lackey et al., 2017); center, methane source pressure of 10,000 kPa, on the order of the largest annular pressure recorded in the Wattenberg Field (Lackey et al., 2017); on the right, methane pressure of 20,340 kPa, the highest pressure for which many casings are rated in Wattenberg Field (Schlumberger, 2014).

temporal evolution of a methane plume, and, at a given k_i, source-zone pressure is the most dominant parameter influencing how much mass is transferred to groundwater.

Parameters describing capillary pressure-saturation or relative permeability-saturation relationships (van Genuchten α and n in these simulations) are important with respect to the amount of methane reaching groundwater, although gas-phase compression limits impacts of these parameters at low values of k_i, as does the range over which α and n are varied. Varying α and n within the range for shale produced negligible changes in the cumulative mass of methane reaching groundwater, whereas varying α from a value associated with silt to a value for shale caused a 3.4% change in the cumulative mass of methane reaching groundwater in the first year after leakage began. Variation of n from a value for silt to a value for shale resulted in a 28% change in the first year of leakage. Predictions associated with the Pierre Shale can be interpreted as conservative estimates (tending to minimize methane migration to groundwater). For a given site, increasing k_i and α and decreasing ϕ and S_L will lead to increasing methane flow rates from wellbore leakage to groundwater as a function of source pressure. The impact of n is dependent on phase saturation due to its inclusion in both the capillary-pressure function and relative-permeability model as a shape parameter. In these simulations, we see an inverse relationship between n and methane reaching groundwater due to increase in aqueous saturation with increasing n. Models with inaccurate multiphase parameterization would be expected to fail to predict changes in capillarity and effective permeability from variations in saturation (e.g., Saiers & Barth, 2012), and, therefore, the mass of methane reaching groundwater.

The scope of the problem is such that millions of kilograms of methane could reach groundwater in the case of a long-term, persistent leak. However, flow rates at the base of the aquifer are slow, and changes in methane concentrations may go undetected. While these results apply generally to low-permeability, unfractured media, limited data for our site (the Pierre Shale in the region of the Wattenberg Field) preclude the model validation necessary to allow actionable conclusions pertaining to an actual leakage event. Application of available technology to evaluate the k_i of formations between groundwater and hydrocarbon production zones and assessing the impact of near-surface fracture networks on methane migration would improve assessment of aquifer vulnerability to hydrocarbon development by informing forecasts of when methane leakage from gas wellbores will reach groundwater and in what volumes, given methane source-zone data. Multiphase modeling of stray-gas migration is an integral part of this analysis, and should be incorporated in future studies of subsurface stray-gas migration. Nonwetting-phase methane gas source pressures and multiphase parameters, which influence capillarity and relative permeability, play a fundamental role in determining volumes and flow rates of methane reaching groundwater and, thus, aquifer vulnerability to methane leakage.

Acknowledgments
The authors acknowledge no conflicting financial support for this work. Data used are from cited references. The code, TOUGH2, is commercially available from http://esd1.lbl.gov/research/projects/tough/ or, with the PetraSim GUI, https://www.thunderheadeng.com/petrasim/

References

Allouche, E. N., Ariaratnam, S. T., Member, A. A., & Lueke, J. S. (2000). Horizontal directional drilling: Profile of an emerging industry. *Journal of Construction Engineering and Management*, *126*, 68–76.

Baihly, J. D., Altman, R. M., Malpani, R., & Luo, F. (2010, September 19–22). *Shale gas production decline trend comparison over time and basins*. Paper presented at SPE-135555-MS SPE Annual Technical Conference and Exhibition, Florence, Italy. https://doi.org/10.2118/135555-MS

Bear, J. (1972). *Dynamics of fluids in porous media*. New York, NY: American Elsevier.

Birdsell, D. T., Rajaram, H., Dempsey, D., & Viswanathan, H. S. (2015). Hydraulic fracturing fluid migration in the subsurface: A review and expanded modeling results. *Water Resources Research*, *51*, 7159–7188. https://doi.org/10.1002/2015WR017810

Bredehoeft, J. D., Neuzil, C. E., & Milly, P. C. D. (1983). *Regional flow in the Dakota aquifer: A study of the role of confining layers* (US Geol. Surv. Water Supply Pap. 2237, 45 p).

Brownlow, J. W., James, S. C., & Yelderman, J. C. Jr. (2016). Influence of hydraulic fracturing on overlying aquifers in the presence of leaky abandoned wells. *Ground Water*, *54*, 781–792. https://doi.org/10.1111/gwat.12431

COGCC (n.d.), *Colorado oil and gas conservation commission, rules and regulations*. Retrieved from http://cogcc.state.co.us/reg.html#/rules, accessed 11 October 2017.

Colorado Geological Survey (CGS) (n.d.), Niobrara calculation tool. Retrieved from http://coloradogeologicalsurvey.org/energy-resources/oil-2/niobrara-calculation-tool/, accessed 20 June 2017.

Colorado Oil and Gas Conservation Commission (COGCC) (2016). Series drilling, development, production and abandonment. Rules & Regu*lations*, 317, GENER, 1–75.

Deutsch, C., & Journel, A. (1998). *GSLIB-geostatistical software library and user's guide*. New York, NY: Oxford University Press.

Digiulio, D. C., & Jackson, R. B. (2016). Impact to underground sources of drinking water and domestic wells from production well stimulation and completion practices in the Pavillion, Wyoming, field. *Environmental Science & Technology*, *50*, 4524–4536. https://doi.org/10.1021/acs.est.5b04970

Drake, R. M., II, Brennan, S. T., Covault, J. A., Blondes, M. A., Freeman, P. A., Cahan, S. M., et al. (2014). Geologic framework for the national assessment of carbon dioxide storage resources—Denver Basin, Colorado, Wyoming, and Nebraska. In P. D. Warwick and M. D. Corum (Eds.), *Geologic framework for the national assessment of carbon dioxide storage resources* (U.S. Geol. Surv. Open-File Rep. 2012–1024–G, 17 p.). Reston, VA: U.S. Geological Survey. http://dx.doi.org/10.3133/ofr20121024G

Dusseault, M. B., Jackson, R. E., & MacDonald, D. (2014). *Towards a road map for mitigating the rates and occurrences of long-term wellbore leakage*. Waterloo, ON: University of Waterloo.

Eltschlager, K. K., Hawkins, J. W., Ehler, W. C., & Baldassare, F. J. (2001). *Technical measures for the investigation and mitigation of fugitive methane hazards in areas of coal mining* (129 p.). Pittsburgh, PA: U.S. Department of the Interior, Office of Surface Mining Reclamation and Enforcement.

Fetkovich, M. J., Vienot, M. E., Bradley, M. D., & Kiesow, U. G. (1987). Decline curve analysis using type curves: Case histories. *SPE Formation Evaluation*, *2*(4), 637–656.

Freeze, R. A., & Cherry, J. A. (1979). *Groundwater*. Englewood Cliffs, NJ: Prentice-Hall.

Gassiat, C., Gleeson, T., Lefebvre, R., & McKenzie, J. (2013). Hydraulic fracturing in faulted sedimentary basins: Numerical simulation of potential contamination of shallow aquifers over long time scales. *Water Resources Research*, *49*, 8310–8327. https://doi.org/10.1002/2013WR014287

Goovaerts, P. (1997). *Geostatistics for natural resources evaluation*. Oxford, NY: Oxford University Press.

Goovaerts, P. (1999). Impact of the simulation algorithm, magnitude of ergodic fluctuations and number of realizations on the spaces of uncertainty of flow properties. *Stochastic Environmental Research and Risk Assessment*, *13*, 161–182. https://doi.org/10.1007/s004770050037

Gorody, A. W. (2012). Factors affecting the variability of stray gas concentration and composition in groundwater. *Environmental Geosciences*, *19*(1), 17–31. https://doi.org/10.1306/eg.12081111013

Higley, D. K., & Cox, D. O. (2007). Oil and gas exploration and development along the front range in the Denver Basin of Colorado, Nebraska, and Wyoming. *In Petroleum systems and assessment of undiscovered oil and Gas in the Denver Basin Province, Colorado, Kansas, Nebraska, South Dakota, and Wyoming—USGS Province 39, U.S. geological survey digital data series* (pp. 1–40). Reston, VA: U.S. Geological Survey.

Howarth, R. W., Santoro, R., & Ingraffea, A. (2011). Methane and the greenhouse-gas footprint of natural gas from shale formations. *Climatic Change*, *106*(4), 679–690. https://doi.org/10.1007/s10584-011-0061-5

Hubbert, M., & Willis, D. (1957). Mechanics of hydraulic fracturing. *Journal for Petroleum Technology*, *9*(6), 153–166. https://doi.org/10.1016/S0376-7361(07)53011-6

Huet, C. C., Rushing, J. A., Newsham, K. E., & Blasingame, T. A. (2005). *A modified Purcell/Burdine model for estimating absolute permeability from mercury-injection capillary pressure data*. Paper presented at International Petroleum Technology Conference (IPTC 10994). Doha, Qatar, 21–23 November.

Ingraffea, A. R., Wells, M. T., Santoro, R. L., & Shonkoff, S. B. C. (2014). Assessment and risk analysis of casing and cement impairment in oil and gas wells in Pennsylvania, 2000–2012. *Proceedings of the National Academy of Sciences of United States of America*, *111*(30), 10955–10960. https://doi.org/10.1073/pnas.1323422111

ISO (1991). ISO Standard 5167, *measurement of fluid flow by means of pressure differential devices—Part 1: Orifice plates, nozzles and venturi tubes inserted in circular cross-section conduits running full*. Geneva, Switzerland: ISO.

Jackson, R. E., Gorody, A. W., Mayer, B., Roy, J. W., Ryan, M. C., & Van Stempvoort, D. R. (2013). Groundwater protection and unconventional gas extraction: The critical need for field-based hydrogeological research. *Ground Water*, *51*(4), 488–510. doi:10.1111/gwat.12074.

Kang, M., Christian, S., Celia, M. A., Mauzerall, D. L., Bill, M., Miller, A. R., et al. (2016). Identification and characterization of high methane-emitting abandoned oil and gas wells. *Proceedings of the National Academy of Sciences of United States of America*, *113*(48), 13636–13641. https://doi.org/10.1073/pnas.1605913113

Kelly, W. R., Matisoff, G., & Fisher, J. B. (1985). The effects of a gas well blow out on groundwater chemistry. *Environmental Geology and Water Sciences*, *7*(4), 205–213. https://doi.org/10.1007/BF02509921

Kissinger, A., Helmig, R., Ebigbo, A., Class, H., Lange, T., Sauter, M., et al. (2013). Hydraulic fracturing in unconventional gas reservoirs: risks in the geological system, part 2. *Environmental Earth Sciences*, *70*(8), 3855–3873. https://doi.org/10.1007/s12665-013-2578-6

Klinkenberg, L. J. (1941). The permeabiliity of porous media to liquids and gases. In *API drilling and production practice* (pp. 200–213). Washington, DC: American Petroleum Institute. https://doi.org/10.5510/OGP20120200114

Lackey, G., Rajaram, H., Sherwood, O. A., Burke, T. L., & Ryan, J. N. (2017). Surface casing pressure as an indicator of well integrity loss and stray gas migration in the Wattenberg Field, Colorado. *Environmental Science and Technology*, *51*(6), 3567–3574. https://doi.org/10.1021/acs.est.6b06071

Ladd, J. H. (2001). An overview and development history of the Wattenberg field. In D. S. Anderson et al. (Eds.), *Gas in the rockies* (pp. 29–42). Denver, CO: Rocky Mountain Association of Geologists.

Lenhard, R. J., Parker, J. C., & Mishra, S. (1989). On the correspondence between Brooks-Corey and van Genuchten models. *Journal of Irrigation and Drainage Engineering*, *115*(4), 744–751.

Llewellyn, G. T., Dorman, F., Westland, J. L., Yoxtheimer, D., Grieve, P., Sowers, T., et al. (2015). Evaluating a groundwater supply contamination incident attributed to Marcellus Shale gas development. *Proceedings of the National Academy of Sciences of United States of America*, *112*(20), 6325–6330. https://doi.org/10.1073/pnas.1420279112

Maxwell, R. M., Carle, S. F., & Tompson, A. F. B. (2008). Contamination, risk, and heterogeneity: On the effectiveness of aquifer remediation. *Environmental Geology*, *54*(8), 1771–1786. https://doi.org/10.1007/s00254-007-0955-8

MIT Energy Initiative (2011). *The future of natural gas: An interdisciplinary MIT study*. Cambridge, MA: MIT Energy Initiative.

Molofsky, L. J., Connor, J. A., Farhat, S. K., Wylie, A. S. Jr., & Wagner, T. (2011). Methane in Pennsylvania water wells unrelated to Marcellus shale fracturing. *Oil and Gas Journal*, *109*(19), 54–67.

Mualem, Y. (1976). A new model for predicting the hydraulic conductivity of unsaturated porous media. *Water Resources Research*, *12*(3), 513–522.

Myers, T. (2012). Potential contaminant pathways from hydraulically fractured shale to aquifers. *Ground Water*, *50*(6), 872–882. https://doi.org/10.1111/j.1745-6584.2012.00933.x

Navarre-Sitchler, A. K., Maxwell, R. M., Siirila, E. R., Hammond, G. E., & Lichtner, P. C. (2013). Elucidating geochemical response of shallow heterogeneous aquifers to CO_2 leakage using high-performance computing: Implications for monitoring of CO_2 sequestration. *Advances in Water Resources*, *53*, 45–55. https://doi.org/10.1016/j.advwatres.2012.10.005

Neuzil, C. E. (1994). How permeable are clays and shales? *Water Resources Research*, *30*(2), 145–150. https://doi.org/10.1029/93WR02930

Nowamooz, A., Lemieux, J.-M., Molson, J., & Therrien, R. (2015). Numerical investigation of methane and formation fluid leakage along the casing of a decommissioned shale gas well. *Water Resources Research*, *51*, 4592–4622. https://doi.org/10.1002/2014WR016146

Oldenburg, C. M., Moridis, G., Spycher, J. N., & Pruess, K. (2004, March). *EOS7C Version 1.0: TOUGH2 module for carbon dioxide or nitrogen in natural gas (methane) reservoirs* (Rep. LBNL-56589, pp. 1–53). Berkeley, CA: Lawrence Berkeley National Laboratory.

Olmstead, S. M., Muehlenbachs, L. A., Shih, J., Chu, Z., & Krupnick, A. J. (2013). Shale gas development impacts on surface water quality in Pennsylvania. *Proceedings of the National Academy of Sciences of United States of America*, *110*(13), 4962–4967. https://doi.org/10.1073/pnas.1213871110

Osborn, S. G., Vengosh, A., Warner, N. R., & Jackson, R. B. (2011). Methane contamination of drinking water accompanying gas-well drilling and hydraulic fracturing. *Proceedings of the National Academy of Sciences of United States of America*, *108*(20), 8172–8176. https://doi.org/10.1073/pnas.1100682108

Peng, D.-Y., & Robinson, D. B. (1976). A new two-constant equation of state. *Industrial & Engineering Chemistry Fundamentals*, *15*(1), 59–64.

Pruess, K., Oldenburg, C., & Moridis, G. (2012). *TOUGH2 user's guide, version 2* (LBNL-43134, November 1999). Berkeley, CA: Lawrence Berkeley National Laboratory.

Reagan, M. T., Moridis, G. J., Keen, N. D., & Johnson, J. N. (2015). Numerical simulation of the environmental impact of hydraulic fracturing of tight/shale gas reservoirs on near-surface groundwater: Background, base cases, shallow reservoirs, short-term gas, and water transport. *Water Resources Research*, *51*, 2543–2573. https://doi.org/10.1002/2014WR016086

Robertson, E. C. (1988). *Thermal properties of rocks* (Open File Rep. 88–441). Reston, VA: U.S. Geological Survey.

Robson, S. G., & Banta, E. R. (1995). *Ground Water Atlas of the United States: Arizona, Colorado, New Mexico, Utah* (Hydrologic Atlas 730, 32 p.). Reston, VA: U.S. Geological Survey. Retrieved from https://pubs.usgs.gov/ha/ha730/ch_c/index.html

Roy, N., Molson, J., Lemieux, J. M., Van Stempvoort, D., & Nowamooz, A. (2016). Three-dimensional numerical simulations ofmethane gas migration from decommissioned hydrocarbon production wells into shallow aquifers. *Water Resources Research*, *52*, 5593–5618. https://doi.org/10.1002/2014WR015716

Saiers, J. E., & Barth, E. (2012). Potential contaminant pathways from hydraulically fractured shale aquifers. *Ground Water*, *50*(6), 826–830. https://doi.org/10.1111/j.1745-6584.2012.00990.x

Scanlon, B. R., Nicot, J. P., & Massmann, J. W. (2002). Soil gas movement in unsaturated systems. In Warrick, A. W. (Ed.), *Soil physics companion* (pp. 297–341). Boca Raton, FL: CRC Press.

Schaap, M. G. (1999). Hydraulic functions used by Rosetta. *Journal of Hydrology*, *251*(3), 163–176.

Schlumberger (2014). *Well services field data handbook* (TSL-1015 V). Houston, TX: Schlumberger. Retrieved from http://www.slb.com/resources/software/ihandbook.aspx

Schultz, L. G., Tourtelot, H. A., Gill, J. R., & Boerngen, J. G. (1980). *Composition and properties of the Pierre shale and equivalent rocks, Northern Great Plains region geochemistry of the Pierre Shale and equivalent rocks of late cretaceous age*.

Schlumberger. (2014). *Well services field data handbook* (TSL-1015 V). Houston, TX. Retrieved from http://www.slb.com/resources/software/ihandbook.aspx

Séjourné, S., Lefebvre, R., Malet, X., & Lavoie, D. (2013). Synthèse géologique et hydrogéologique du Shale d'Utica et des unités sus-jacentes (Lorraine, Queenston et dépôts meubles), Basses-Terres du Saint-Laurent, Province de Québec; Open file 7338. *Commission Géologique du Canada*, *7338*, 1–165. https://doi.org/10.4095/292430

Sherwood, O. A., Rogers, J. D., Lackey, G., Burke, T. L., Osborn, S. G., & Ryan, J. N. (2016). Groundwater methane in relation to oil and gas development and shallow coal seams in the Denver-Julesburg Basin of Colorado. *Proceedings of the National Academy of Sciences of United States of America*, *113*(30), 8391–8396. https://doi.org/10.1073/pnas.1523267113

Stone, C. H., Fleckenstein, W. W., & Eustes, A. W. (2016). *SPE-181696-MS: An assessment of the probability of subsurface contamination of aquifers from oil and gas wells in the Wattenberg Field, modified for water well location* (Figure 1, pp. 1–23).

Survey (COGS), C. G. (n.d.). Niobrara calculation tool. Retrieved from http://coloradogeologicalsurvey.org/energy-resources/oil-2/niobrara-calculation-tool/

van Genuchten, M. T. (1980). A closed-form equation for predicting the hydraulic conductivity of unsaturated soils. *Soil Science Society of America Journal*, *44*(5), 892–898. https://doi.org/10.2136/sssaj1980.03615995004400050002x

Van Stempvoort, D., Maathuis, H., Jaworski, E., Mayer, B., & Rich, K. (2005). Oxidation of fugitive methane in ground water linked to bacterial sulfate reduction. *Ground Water*, *43*(2), 187–199. https://doi.org/10.1111/j.1745-6584.2005.0005.x

Tanikawa, W., & Shimamoto, T. (2006). Klinkenberg effect for gas permeability and its comparison to water permeability for porous sedimentary rocks. *Hydrology and Earth System Sciences Discussions*, *3*(4), 1315–1338. https://doi.org/10.5194/hessd-3-1315-2006

US Department of Energy (DOE) (2009). *Modern shale gas development in the United States: A primer*. Washington, DC: U.S. Department of Energy (DOE).

US Energy Information Administration (EIA) (2014). *Annual Energy Outlook 2014 with projections to 2040*). Washington, DC: DOE-EIA.

US Energy Information Administration (EIA) (2015). *Annual Energy Outlook 2015 with projections to 2040*). Washington, DC: DOE-EIA.

US Energy Information Administration (EIA) (2016). *Annual Energy Outlook 2016 with projections to 2040*. Washington, DC: DOE-EIA.

US Environmental Protection Agency—US EPA (2016). *EPA on-line tools for site assessment calculation*. Retrieved from: https://www3.epa.gov/ceampubl/learn2model/part-two/onsite/tempmap.html, accessed 4 April 2017.

Vengosh, A., Jackson, R. B., Warner, N., Darrah, T. H., & Kondash, A. (2014). A critical review of the risks to water resources from unconventional shale gas development and hydraulic fracturing in the United States. *Environmental Science & Technology*, *48*(15), 8334–8348. https://doi.org/10.1021/es405118y

Vidic, R. D., Brantley, S. L., Vandenbossche, J. M., Yoxtheimer, D., & Abad, J. D. (2013). Impact of shale gas development on regional water quality. *Science*, *340*(6134), 1235009. https://doi.org/10.1126/science.1235009

Wang, F. P., & Reed, R. M. (2009). Pore networks and fluid flow in gas shales. In *SPE Annual Technical Conference and Exhibition*, New Orleans, Louisiana, USA (SPE 124253). https://doi.org/10.2118/124253-MS

Warner, N. R., Jackson, R. B., Darrah, T. H., Osborn, S. G., Down, A., Zhao, K., White, A., & Vengosh, A. (2012). Geochemical evidence for possible natural migration of Marcellus Formation brine to shallow aquifers in Pennsylvania. *Proceedings of the National Academy of Sciences of United States of America*, *109*(30), 11961–11966. https://doi.org/10.1073/pnas.1121181109

Watson, T. L., & Bachu, S. (2009). Evaluation of the potential for gas and CO_2 leakage along wellbores. *SPE Drilling & Completion*, *24*, 115–126. https://doi.org/10.2118/106817-PA

Weimer, R. J., & Sonnenberg, S. A. (1996). *Guide to the petroleum geology and Laramide Orogeny, Denver Basin and Front Range, Colorado* (Vol. 51, 127 p.). Golden, CO: Department of Natural Resources, Colorado Geological Survey.

Wu, Y., Pruess, K., Persoff, P., Division, E. S., & Berkeley, L. (1998). Gas flow in porous media with Klinkenberg effects. *Transport in Porous Media*, *32*, 117–137. https://doi.org/10.1023/A:1006535211684